8-20-1991

Mie Theory Model of the Corona

James A. Lock
Cleveland State University, j.lock@csuohio.edu

Leiming Yang

Original Citation

Lock, James A. and Leiming Yang*. "Mie Theory Model of the Corona." *Applied Optics* 30 (1991): 3408-3414.

Mie theory model of the corona

James A. Lock and Leiming Yang*

We performed a calculation of the corona colors that employed Mie theory to obtain the scattered light intensity. The scattered intensity was integrated over the visible spectrum for a number of different cloud droplet size distriubtions. The results were converted to chromaticity coordinates, convolved with the angular size of the sun, and plotted on the 1931 CIE chromaticity diagram. The results were compared to observations of multiple-ring coronas. It was found that, when using Mie theory to estimate cloud droplet sizes, water droplets with diameters in the 7-μm $\lesssim D \lesssim$ 15-μm range produced the 13 multiple-ring coronas that were observed.

I. Introduction

The corona is a sequence of concentric pink and pale green rings of light that are occasionally seen around the sun or moon when observed through a thin layer of altocumulus or cirrocumulus clouds[1–3] (see Plate 8). This phenomenon is not to be confused with the portion of the solar atmosphere that bears the same name. The standard model employed in the explanation of the corona is the diffraction of the sunlight or moonlight by the nearly monodisperse population of water droplets that comprise the cloud.[2,4,5] The pink rings are the most apparent features of the corona, and in the diffraction model their angular radii θ_N are given by[6]

$$\sin\theta_N = (N + 0.22)\lambda_G/D, \tag{1}$$

where D is the diameter of the cloud droplets and N is an integer that denotes the order of the colored band. The wavelength $\lambda_G = 0.57$ μm is commonly chosen because the pink corona rings appear most vivid at the angles for which the diffracted green light is absent.[6,7]

A more accurate model of the corona is provided by Mie theory. The Mie scattering amplitudes may be written in the form of a sum whose terms may be interpreted as diffraction, specular reflection, transmission, and transmission following an arbitrary number of internal reflections. The processes of transmission and diffraction cause interference in the near-forward direction, and, as a result, the intensity and spacing of the Mie scattering maxima and minima differ from the results of diffraction alone. This diffraction-plus-transmission mechanism has been called anomalous diffraction.[8] It is of interest to determine the consequences of this interference in the context of Mie theory on the observability of the corona.[9,10] In addition, water droplets within a cloud have a wide range of diameters, each producing a different angular scattering pattern. The observed corona is an incoherent average over these different patterns, and the averaging process washes out the colors of the rings and decreases their visibility. It is of interest to determine how wide the cloud droplet size distribution must be before the contrast of the colors of the corona rings is decreased to such an extent that they are no longer observable.

In Section II we quickly review the diffraction model of the corona and relate various properties of the corona to the chromaticity curve. In Section III we perform a Mie theory calculation of the corona and obtain the chromaticity coordinates of the scattered light as functions of the angle from the sun. The chromaticity coordinates are plotted on the 1931 CIE chromaticity diagram. In Section IV we describe observations of a number of multiple-ring coronas, and in Section V our results are compared to these observations.

Similar chromaticity calculations have been performed for the rainbow and its supernumeraries[11] and for light reflected from a thin film of soapy water.[12] We believe that a chromaticity calculation has not been undertaken previously for the corona,[13] although calculations of various properties of the corona employing Mie theory have been performed.[14–16]

The authors are with Department of Physics, Cleveland State University, Cleveland, OH 44115.

Received 1 October 1990.
0003-6935/91/243408-07$05.00/0.

II. Diffraction Model of the Corona

We consider unpolarized light from a point source that is deflected through an angle θ by a single cloud water droplet of diameter D. The jth chromaticity coordinate of the deflected light as a function of θ is given by[17]

$$r_j(\theta) = \frac{\int d\lambda I(D, \lambda, \theta)\bar{r}_j(\lambda)b(\lambda)}{\sum_{k=1}^{3}\int d\lambda I(D, \lambda, \theta)\bar{r}_k(\lambda)b(\lambda)}, \quad (2)$$

where $(r_1, r_2, r_3) = (x, y, z)$, $I(D, \lambda, \theta)$ is the deflected light intensity, and $\bar{r}_j$ is the equal-energy stimulus coefficient[18] for wavelength λ for $j = 1,2,3$. We take $b(\lambda)$ to be the blackbody irradiance of the sun even though we are presently considering a point source, and the integration with respect to wavelength extends over the visible spectrum. Chromaticity coordinates near the center of the 1931 CIE chromaticity diagram correspond to unsaturated colors and appear nearly white. Points near the edge of the diagram correspond to colors that are almost completely saturated and appear similar to pure spectral colors.

In the diffraction model of the corona, the diffracted intensity is

$$I(D, \lambda, \theta) = \frac{I_0 X^2 D^2}{4R^2}\left[\frac{J_1(X\theta)}{X\theta}\right]^2, \quad (3)$$

where the size parameter of the droplet is

$$X \equiv \frac{\pi D}{\lambda}, \quad (4)$$

R is the distance from the droplet to the observer, and I_0 is a normalization constant. Substituting Eq. (3) into Eq. (2) gives

$$r_j(v) = \frac{\int d\lambda \bar{r}_j(\lambda)b(\lambda)\left[\frac{J_1(\pi v/\lambda)}{\pi v/\lambda}\right]^2}{\sum_{k=1}^{3}\int d\lambda \bar{r}_k(\lambda)b(\lambda)\left[\frac{J_1(\pi v/\lambda)}{\pi v/\lambda}\right]^2}, \quad (5)$$

where

$$v \equiv D\theta. \quad (6)$$

The chromaticity coordinates of Eq. (5) depend on the cloud droplet diameter and on the scattering angle θ only with the parameter v of Eq. (6). As a consequence, the shape of the chromaticity curve for each diameter droplet is identical except for a scaling of the scattering angle, and droplets of all sizes produce equally observable corona rings in the diffraction model. This statement is only true for point-source illumination. The 0.5° diameter of the sun would render closely spaced corona rings less observable than ones with a greater spacing.

The chromaticity curve for Eq. (5) is shown in Fig. 1. (For readers unfamiliar with the 1931 CIE chromaticity diagram, a readable account of it is given in Chap. 9 of Ref. 19.) In this figure, after the first cycle of the curve, its orientation changes from blue-to-red to green-to-red. This change in orientation is possibly

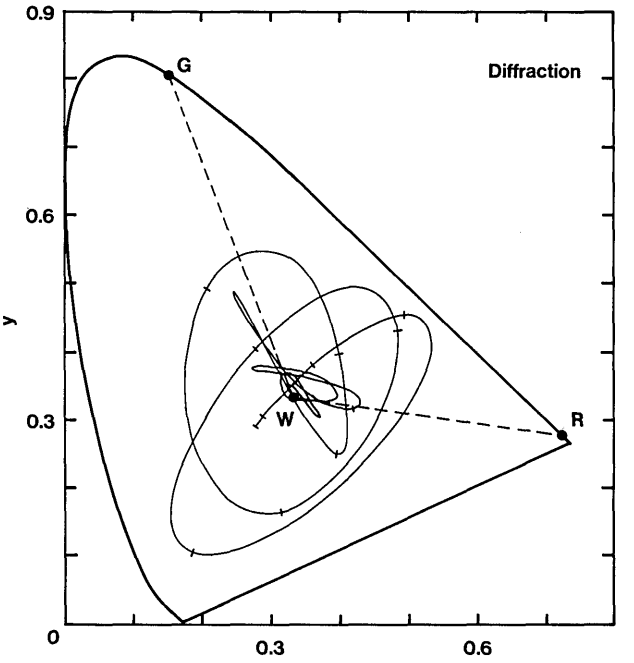

Fig. 1. Chromaticity curve for the corona of Eq. (5) in the diffraction model. Point W = (0.333, 0.333) is the equal-energy white point and points R and G are primary spectral red (0.65 μm) and green (0.53 μm). The lines joining R to W and G to W denote various saturations of red and green, respectively. We take the intersections of these lines and the chromaticity curve to represent the red and green corona rings. The grid marks on the chromaticity curve are at intervals of $\Delta v = 10.0$ μm deg.

the reason the corona rings appear pink and pale green. The same change in orientation of the chromaticity curve occurs for the light reflected from a thin film of soapy water.[12] The large background illumination near the sun has not been taken into account in Fig. 1.

In Fig. 1, lines joining equal-energy white (W: $x = y = 0.333$) with primary spectral green[19] (G: $\lambda = 0.53$ μm) and primary spectral red (R: $\lambda = 0.65$ μm) have been drawn on the chromaticity diagram. The chromaticity curve intersects these lines a number of times. We take the distances

$$\Delta r = [(\Delta x)^2 + (\Delta y)^2]^{1/2} \quad (7)$$

from the intersection points to point W as a measure of the purity of color, or the distinguishability from white, of the red and green corona rings. MacAdam[20] and Wright[21] have measured the color distinguishability threshold for closely spaced locations on the chromaticity diagram. They found that, for near-ideal conditions, along the primary red line (RW) near W, the color distinguishability threshold is $\Delta r \approx 0.007$, while along the primary green line (GW) near W the threshold is larger, $\Delta r \approx 0.015$. When these threshold purity differences Δr are divided by the lengths of the lines RW and GW, respectively, the ratio is also larger for green than for red.[22] The lower threshold for observable differences in red is possibly the reason the

red rings are commonly said to be the dominant observed feature of the corona.[23]

For observations made close to the direction of the sun, it is unlikely that the color distinguishability threshold for the corona rings is as small as $\Delta r \approx 0.007$. The observation of the corona around the sun is made much easier by blocking the position of the sun and looking through tinted glass, or looking at the corona's reflection in a puddle of water. These techniques serve to decrease the background illumination near the sun and thus increase the color distinguishability threshold. For this method of observation, if $\Delta r \approx 0.007$ were realistic for the red corona rings, one would expect that, in the diffraction model, as many as about eight red rings could be observed. The largest number of red corona rings that has been reported is five,[24,25] and it is unusual that more than two are seen. As a result, it is possible that the diffraction model overestimates the purity of the colors of the corona rings.

III. Mie Theory Model of the Corona

To examine this possibility, the Mie theory calculation of the corona colors described here was undertaken. We used a blackbody temperature of the sun of 5700 K to obtain $b(\lambda)$. The wavelength dependence of the refractive index of water was parametrized by

$$n(\lambda) = 1.3271 + 0.0019/\lambda^2, \tag{8}$$

where λ is measured in micrometers. This parametrization closely fits the data of Ref. 26. The Mie intensity for unpolarized light scattered by a single water droplet,

$$I_{\mathrm{Mie}}(D, \lambda, \theta) = \frac{I_0 D^2}{8X^2R^2}\left[|S_1(X, \theta)|^2 + |S_2(X, \theta)|^2\right], \tag{9}$$

was computed using the program[27] BHMIE for 61 evenly spaced wavelengths in the $0.4\text{-}\mu\mathrm{m} \le \lambda \le 0.7\text{-}\mu\mathrm{m}$ interval for scattering angles at intervals of $\Delta\theta = 0.125°$. The scattered intensity was used in Eq. (2) to calculate the chromaticity coordinates of the light scattered by a single droplet as functions of the angle from the sun. The two-dimensional convolution of the chromaticity coordinates over the disk of the sun was approximated by the one-dimensional convolution

$$r_j^{\mathrm{conv}}(\theta) = \int_{-\theta_{\max}/2}^{\theta_{\max}/2} \mathrm{d}\theta' \left(1 - \frac{\theta'^2}{\theta_{\max}^2}\right)^{1/2} r_j(\theta - \theta'), \tag{10}$$

where $\theta_{\max} = 0.5°$. Again, the large background illumination near the sun was not included in the results, corresponding to the method of observation described at the end of Section II.

The convolved chromaticity curves showed a large degree of variability for different diameter water droplets. For single droplets with $D \lesssim 7\mu\mathrm{m}$, the curves did not possess a well-defined cycling behavior. They also changed greatly for small changes in D. A representative chromaticity curve of this type is shown in Fig. 2(a). For $7\ \mu\mathrm{m} \lesssim D \lesssim 17\mu\mathrm{m}$, the curves exhibited an increasingly well-defined cycling behavior. They also changed much more slowly as D was varied. As an example, the chromaticity curve for $D = 14\ \mu\mathrm{m}$ is shown in Fig. 2(b). Lastly, for $D \gtrsim 17\ \mu\mathrm{m}$, the shape of the chromaticity curve became virtually independent of D as was the case for all droplet diameters in the diffraction model. The chromaticity curve for $D = 21\ \mu\mathrm{m}$ is shown in Fig. 2(c).

These convolved chromaticity curves exhibit a number of interesting features. First, in Figs. 2(b) and 2(c), the curve spirals inward toward W at a faster rate than it does in Plate 1 for the diffraction model. As a result, fewer red rings are expected to be observable on the basis of the Mie theory model. Second, the lack of a simple behavior of the chromaticity curve in Fig. 2(a) reflects the irregularities in the near-forward Mie intensity produced by the interference between diffraction and transmission components of the Mie amplitudes. For small scattering angles, the magnitudes of the relative maxima and minima of the Mie intensity oscillate in an irregular fashion because of the diffraction–transmission interference with a period of $\Delta X \approx 3$. The range of size parameters integrated in Eq. (2) is $\Delta X \approx 3.3D$. Thus for small diameter droplets, ΔX is small, only a few irregularities of the maxima and minima are integrated, and their presence strongly biases the resulting chromaticity coordinates. For large diameter droplets, ΔX is large, many irregularities are integrated, and their biases tend to cancel.

The color purity Δr of the red rings (i.e., the distances on the chromaticity diagram along the RW line from W to the intersections with the convolved chromaticity curve) is given in Fig. 3 as a function of water droplet diameter. From this figure we see that some diameter droplets produce red corona rings with greater purity than do other diameter droplets. A dependence of observability on droplet size has previously been found for supernumerary rainbows[28] and glories.[29] If we equate color purity and distinguishability from white with observability, the dependence here is oscillatory with the period $\Delta D \approx 2\ \mu\mathrm{m}$. When the width of the droplet size distribution in the cloud is of the order of ΔD or greater, droplets producing more vividly colored and less vividly colored rings are averaged together producing approximately equal vividness for all size distributions of a given width, independent of the average droplet diameter. This averaging property for wide distributions is reminiscent of the droplet-independent observability that was found in the diffraction model.

To investigate the effect of the size distribution in greater detail, we took the number of water droplets with a diameter between D and $D + \mathrm{d}D$ to be $N(D)\mathrm{d}D$. The chromaticity coordinate $r_j(\theta)$ of the light scattered by this distribution of droplets is given by

$$r_j(\theta) = \frac{\int \mathrm{d}D \int \mathrm{d}\lambda N(D) I(D, \lambda, \theta) \bar{r}_j(\lambda) b(\lambda)}{\sum_{k=1}^{3} \int \mathrm{d}D \int \mathrm{d}\lambda N(D) I(D, \lambda, \theta) \bar{r}_k(\lambda) b(\lambda)}. \tag{11}$$

Although realistic droplet size distributions in clouds are approximately lognormal, for simplicity we employed the idealized size distribution

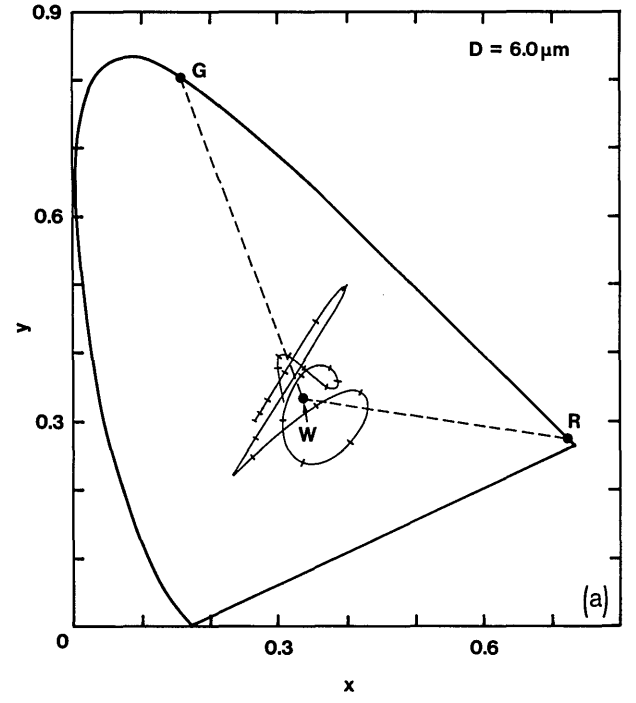

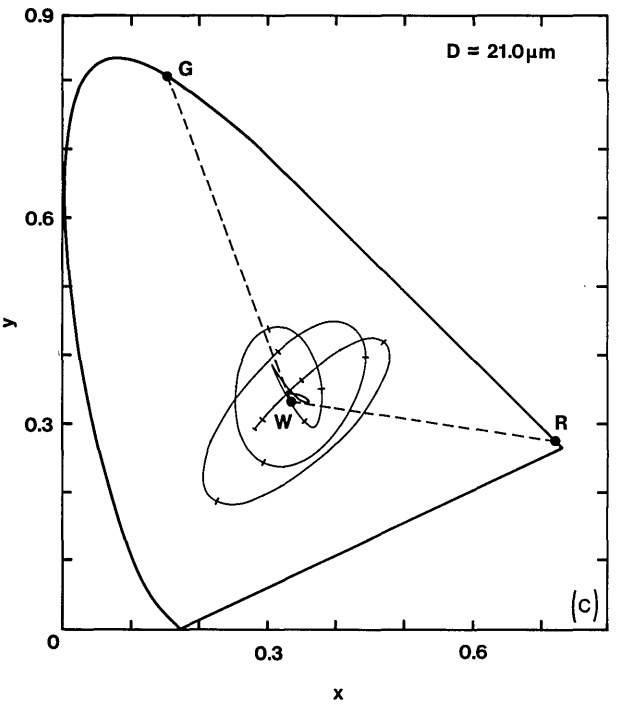

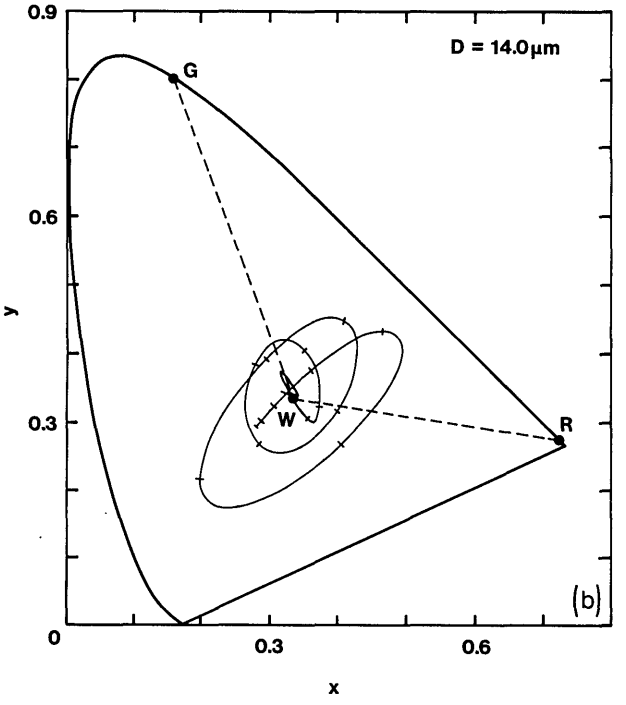

Fig. 2. Convolved chromaticity curve for the corona in the Mie theory model for (a) $D = 6.0\ \mu m$, (b) $D = 14.0\ \mu m$, and (c) $D = 21.0\ \mu m$. Points W, R, and G are as in Fig. 1. The grid marks on the chromaticity curve are at intervals of $\Delta\theta = 1.0°$ in (a) and $\Delta\theta = 0.5°$ in (b) and (c).

$$N(D) = \begin{cases} N_0 & \text{if } D_0 - w/2 \le D \le D_0 + w/2, \\ 0 & \text{otherwise} \end{cases} \tag{12}$$

in Eq. (11) where D_0 is the average droplet diameter and w is the width of the distribution. As expected, the resulting convolved chromaticity curves showed a smaller degree of saturation than did the convolved single droplet curves. A representative example is shown in Fig. 4 for $D_0 = 14.0\ \mu m$ and $w = 4.0\ \mu m$. The color purity Δr of the red rings was determined as a function of the distribution width w and is given in Fig. 5 for the second, third, and fourth red rings for $D_0 = 8$, 14, and 21 μm. For $D_0 = 8\ \mu m$, again neglecting the large background light near the sun, if the width of the size distribution is greater than $\sim 2\ \mu m$, the second and third red rings should not be observable and only the interior aureole red ring should be seen. On the other hand, for $D_0 = 21\ \mu m$, multiple red rings should be observable until the distribution becomes $\sim 8\ \mu m$ wide.

The aureole or first red ring prominently appears in

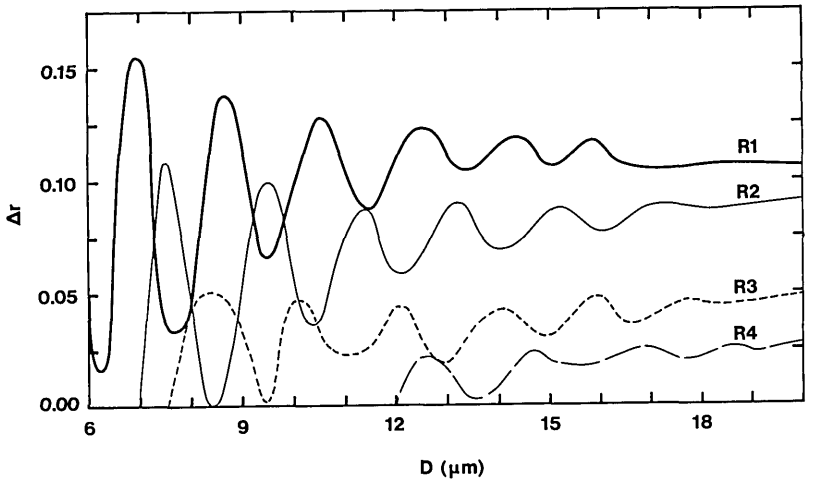

Fig. 3. Purity of the color of the first four red corona rings, R1 through R4, as a function of water droplet diameter in the Mie theory model.

the chromaticity diagrams for all the droplet diameters and size distributions that we examined. Thus the observed absence of even the aureole probably results from multiple scattering within an optically thick cloud. Multiple scattering was not included in our calculations, and as a result the visibility of the second through the fourth red rings should be poorer for optically thick clouds than Fig. 5 would indicate. But for the extensive altocumulus and orographically induced altocumulus standing lenticular clouds in which multiple coronas are most often observed, the cloud thickness is often <100 m and multiple scattering is expected to be relatively unimportant.[30]

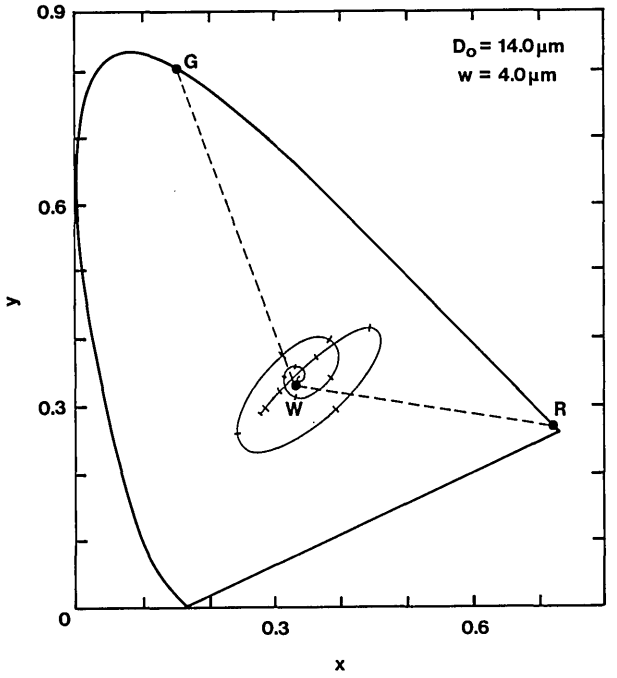

Fig. 4. Convolved chromaticity curve for the corona in the Mie theory model for $D_0 = 14.0\ \mu m$ and $w = 4.0\ \mu m$. Points W, R, and G are as in Fig. 1. The grid marks on the chromaticity curve are at intervals of $\Delta\theta = 0.5°$.

Observations of the corona have long been employed to estimate the dominant diameter of the droplets within the corona-producing cloud. Previous estimates have been made using Eq. (1) of the diffraction model with $\lambda_G = 0.57\ \mu m$. In the current calculation, the scattering angles at which the chromaticity curves for monodisperse droplets intersected the RW line were calculated and are shown in Fig. 6 as a function of droplet diameter. For the size distribution of Eq. (12), the angular positions of the various red rings were found to be virtually the same as for the dominant diameter D_0 alone. As has been pointed out before,[9,14] Fig. 6 shows that the diffraction model with $\lambda_G = 0.57\ \mu m$ overestimates the droplet diameter. For small diameters, the Mie theory results become erratic because of diffraction–transmission interference effects. The Mie theory model results of Fig. 6 may be reasonably approximated by the simpler Eq. (1) using $\lambda_G = 0.490\ \mu m$.

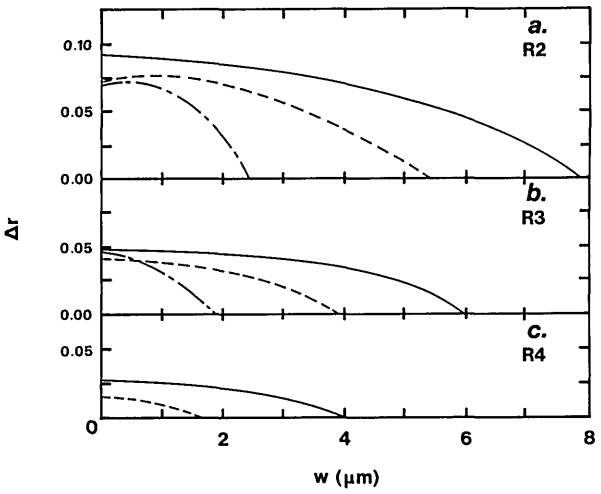

Fig. 5. Purity of the color of the second through fourth red corona rings, R2 through R4, as a function of the size distribution width w. The solid curve is $D_0 = 21.0\ \mu m$, the dashed curve is $D_0 = 14.0\ \mu m$, and the dot-dash curve is $D_0 = 8.0\ \mu m$.

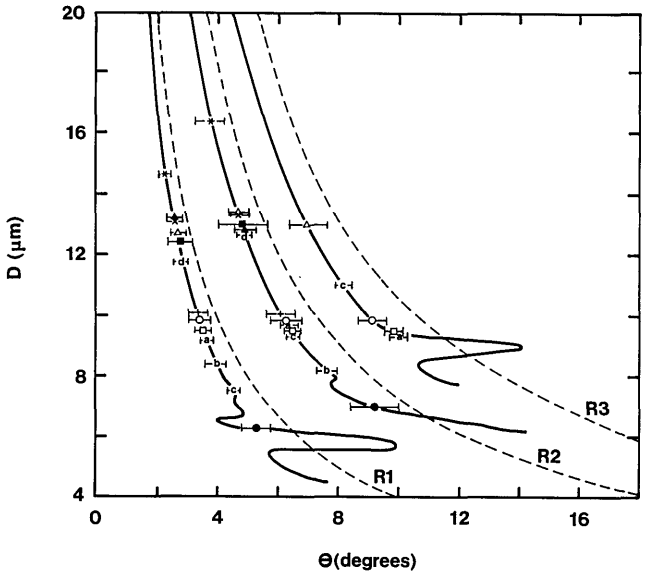

Fig. 6. Water droplet diameter as a function of the angular radius θ of the first three red corona rings. The solid curve is the prediction of the Mie theory model and the dashed curve is the prediction of the diffraction model with $\lambda_G = 0.57$ μm. Open circle data points, 22 Aug. 1989; solid circle, 20 Dec. 1989; solid square, 14 Jan. 1990; solid triangle, Ref. 30; open triangle, Ref. 31. The X's denote Fraser's photographic observations of 6 Dec. 1969; open squares, 20 Jan. 1971; pluses, 23 Jan. 1971; stars, 19 Apr. 1971. The a points are Sassen's photographic observations of 24 Mar. 1976; b, Nov. 1974; c, Feb. 1978; d, June 1977.

IV. Observations

During the period from August 1989 to February 1990, the authors photographed and analyzed three coronas containing at least two partial red rings. A colorimetric analysis of the photographs was not undertaken.[31] Instead, the positions of the red rings were estimated as the locations where the red color appeared the most vivid. The error in the angular diameters obtained in this way is comparable with the error caused by the noncircularity of the rings in some of the photos, which resulted from the nonuniformity of the droplet size distribution near the edges of the cloud. We also estimated the angular radii of the red rings in two published photographs of coronas containing at least two partial red rings[32,33] and in photographs of eight additional coronas that were kindly provided by A. Fraser and K. Sassen. These data are also shown in Fig. 6.[34,35]

V. Discussion

Assuming that the Mie theory model gives the exact correspondence between droplet diameter and the radii of the red rings, the diameters of the droplets producing multiple-ring coronas may be estimated using Fig. 6. The presumed correspondence between the angular radius and droplet diameter indicates that, although altocumulus clouds can contain water droplets in a large range of sizes,[36] the dominant sizes of the cloud droplets responsible for multiple-ring coronas fall within a narrow range.

The fact that no multiple-ring coronas were produced by cloud droplets less than ~6.5-μm diameter is compatible with the lack of simplicity of the chromaticity curve found in Secton III for $D_0 \lesssim 7$ μm. However, iridescence is commonly observed in clouds with droplet diameters much smaller than this limit. It is interesting that no $D_0 \gtrsim 15$-μm multiple-ring coronas[34] were observed despite the large population of droplets of these diameters that can be present in altocumulus clouds.[36] If our observations of multiple-ring coronas are representative, this absence possibly indicates that, as an altocumulus cloud evolves, either its droplet size distribution remains rather narrow until $D_0 \approx 14$ μm, at which point the distribution broadens rapidly, or that the cloud becomes optically thick at this point and multiple scattering obscures the rings. Independent measurements of droplet size distributions in altocumulus clouds as they evolve and multiple-scattering calculations are necessary to determine whether either of these explanations of the absence of multiple-ring coronas produced by large diameter droplets is correct.

The authors thank K. Sassen for providing us with copies of the papers of Simpson, Bricard, and Naik, suggesting the new value for λ_G, and for providing us with his collection of corona photographs. We also thank A. Fraser for providing us with his collection of corona photographs and for several helpful comments on an earlier version of this manuscript.

*Present address, Department of Physics, New Mexico State University, Las Cruces, New Mexico 88003.

References

1. M. Minnaert, *Tne Nature of Light and Colour in the Open Air* (Dover, New York, 1954), articles 160 and 161.
2. R. A. R. Tricker, *Introduction to Meteorological Optics* (American Elsevier, New York, 1970), Chap. 5.
3. R. Greenler , *Rainbows, Halos, and Glories* (Cambridge U. Press, Cambridge, England, 1980), Chap. 6.
4. W. J. Humphreys, *Physics of the Air* (Dover, New York, 1964), Chap. 6.
5. C. Bohren, "A serendipitous iridescent cloud," Weatherwise **38**, 268–274 (1985).
6. G. C. Simpson, "Coronas and iridescent clouds," Q. J. R. Meteorol. Soc. **38**, 291–301 (1912).
7. H. C. van de Hulst, *Light Scattering by Small Particles* (Dover, New York, 1981), p. 425.
8. Ref. 7, Sections 11.22, 11.3, and 13.41.
9. J. G. Wilson, "Note on optical methods of measuring the size of small water drops," Proc. Cambridge Philos. Soc. **32**, 493–498 (1936).
10. J. Bricard, "Reflexion, refraction et diffraction de la lumiere par une goutte d'eau spherique," Ann. Geophys. **2**, 231–248 (1946).
11. J. A. Prins and J. J. M. Reesnick, "Buigingstheorie en trichromatische specificatie van de Regenboogkleuren," Physica **11**, 49–60 (1944).
12. J. D. Walker, "The bright colors in a soap film are a lesson in wave interference," Sci. Am. **239**(3), 232–237 (1978).

13. Ref. 7, p. 425, appears to be in error on this point. The calculations of Prins and Reesinck and of Buchwald are for the rainbow, not for the corona.
14. Y. G. Naik, "Correlation between optical and dynamic methods of measuring size of water drops in a cloud," J. Colloid Sci. **9**, 393–399 (1954).
15. Ref. 7, Fig. 52.
16. K. Sassen, "Iridescence in an aircraft contrail," J. Opt. Soc. Am. **69**, 1080–1083 (1979).
17. R. W. Burnham, R. M. Hanes, and C. J. Bartleson, *Color: A Guide to Basic Facts and Concepts* (Wiley, New York, 1963), pp. 130–133.
18. W. D. Wright, *The Measurement of Colour* (Hilger, London, 1969), Appendix 2, Table 4.
19. D. Falk, D. Brill, and D. Stork, *Seeing the Light* (Harper & Row, New York, 1986), p. 244.
20. D. L. MacAdam, "Visual sensitivities to color differences in daylight," J. Opt. Soc. Am. **32**, 247–274 (1942).
21. Ref. 18, Fig. 6.3.
22. C. F. Bohren, "Understanding colors in nature," Pigment Cell Res. **1**, 214–222 (1988).
23. Ref. 1, p. 215.
24. Ref. 1, p. 214.
25. Ref. 2, p. 146.
26. E. J. McCartney, *Optics of the Atmosphere* (Wiley, New York, 1976), Table 5.3.
27. C. F. Bohren and D. R. Huffman, *Absorption and Scattering of Light by Small Particles* (Wiley, New York, 1983), Appendix A.
28. A. B. Fraser, "Why can the supernumerary bows be seen in rain showers," J. Opt. Soc. Am. **73**, 1626–1628 (1983).
29. J. A. Lock, "Observability of atmospheric glories and supernumerary rainbows," J. Opt. Soc. Am. A **6**, 1924–1930 (1989).
30. S. D. Gedzelman, "In praise of altocumulus," Weatherwise **41**, 143–149 (1988).
31. For a colorimetric analysis of rainbow photographs see R. L. Lee, "What are 'all the colors of the rainbow'?" Appl. Opt. **30**, 3401–3407 (1991).
32. H. Lansford, "Shooting the sky," Weatherwise **35**, 73–81 (1982).
33. S. J. O'Meara, "Yellowstone: a natural phenomenon," Sky Telesc. **70**, 369 (1985).
34. The data of Fig. 6, where different diameter droplets correspond to different red rings in a single corona, resulted from the corona occurring at the edge of the cloud where the droplet size distribution was not homogeneous.
35. One additional corona photograph provided by K. Sassen was analyzed for which Fig. 6 predicts a droplet diameter of 21 μm. This corona, however, occurs in a cirrostratus cloud and possesses a number of the features particular to ice crystal coronas. see for example, K. Sassen, "Corona-producing cirrus cloud properties derived from polarization lidar and photographic analyses," Appl. Opt. **30**, 3421–3428 (1991).
36. Ref. 26, Table 3.6.